



Enhance controllability of a memristive neuron under magnetic field and circuit approach

Feifei Yang^{1,2}, Zhitang Han³, Guodong Ren^{2,a} , Qun Guo¹, Jun Ma^{1,2}

¹ College of Electrical and Information Engineering, Lanzhou University of Technology, Lanzhou 730050, China

² Department of Physics, Lanzhou University of Technology, Lanzhou 730050, China

³ School of Information Science and Engineering, Dalian Polytechnic University, Dalian 116034, China

Received: 9 April 2024 / Accepted: 13 June 2024

© The Author(s), under exclusive licence to Società Italiana di Fisica and Springer-Verlag GmbH Germany, part of Springer Nature 2024

Abstract A quiescent neuron develops static electric field in the media beside two sides of the cell membrane. In presence of external electric stimuli or electromagnetic radiation, the neurons can be excited to induce time-varying electric field and magnetic field during continuous pumping of intracellular ions. When external magnetic field is applied to the media, the ions propagation across the ion channels are affected and the firing patterns are changed. In this paper, a magnetic flux-controlled memristor (MFCM) is connected into a FitzHugh–Nagumo (FHN) neural circuit to build a memristive circuit, and its equivalent memristive neuron can perceive the modulation from external magnetic field. The circuit equations are obtained under Kirchhoff's law and field energy function for the neural circuit is defined, and then scale transformation is applied to obtain its equivalent neuron model and dimensionless energy function. The Hamilton energy function for this memristive neuron can also be obtained by using the Helmholtz theorem. In addition, an adaptive growth law of for memristive channel gain is presented to express the self-adaptive property in of the memristive neuron. Dynamic analysis indicates that the memristive neuron can be induced complex firing patterns (bursting, spiking and chaotic) by changing the external stimuli and external magnetic field. The simulation result of the Multisim software illustrates that the memristive neuron can be realized by applying analog circuit.

1 Introduction

Memristor explains the relationship between charge and magnetic flux, in 1971, Chua [1] firstly proposed the concept of memristor. Memristors are usually divided into two categories: charge-controlled memristor (CCM) [2–4] and MFCM [5–7]. Chaotic circuit is an important research content in nonlinear circuits, and the nonlinear element is the key for designing chaotic circuits. Memristor is widely used in the field of chaotic circuits because of the nonlinear characteristic and its controllability under external electromagnetic field. For example, Chen et al. [8] designed a mix chaotic circuit by applying a memristor, a capacitor, an induction coil and a memcapacitor. Luo et al. [9] obtained an improved memristive chaotic circuit by replacing the Chua diode in the Chua circuit with a memristor. Peng et al. [10] proposed a new memristive chaotic circuit by replacing the nonlinear term in the Chua circuit with a memristor and a negative conductance. Wang et al. [11] introduced a chaotic circuit by applying an extended memristor and a capacitor. In Ref. [12], a 5D Wien-bridge hyperchaotic memristive circuit was developed from a 4D Wien-bridge chaotic circuit. Memristors have also been studied in discrete maps by introducing different kinds of memristive terms into the mathematical maps. For instance, 2D memristive chaotic maps [13–15], 2D memristive hyperchaotic maps [16–18], 3D memristive chaotic maps [19, 20], 3D memristive hyperchaotic maps [21–23], 4D memristive map [24], higher dimensional memristive map [25] and memristive neuron maps [26–30].

Because the electrical properties of memristors are similar to synapses work [31, 32], memristors are used to simulate the synapses of biological neurons. For instance, Yang et al. [33] investigated the activation and connection of synapses by coupling two functional neurons via memristors. Guo et al. [34] coupled two photoelectric neurons by applying memristive synapse, and explored the synchronization between neurons. Wu et al. [35] confirmed that a memristive synapse can produce similar firing patterns in a neuron encoded with chemical synapse. Hou et al. [36] studied the effect of energy flow on mode selection in neural activities and stochastic resonance in a memristive neuron. In Refs. [37, 38], a memristive neuron was proposed to estimate the external electric field and electromagnetic field, and the self-adaptive regulation mechanism in neural activities under energy flow is explained [39]. In fact, the involvement of Josephson junction [40–44] and other functional electric components [45–49] enable the neural circuits to detect different physical stimuli effectively. Based on these memristive models, the coupling channels and links are tamed to create a variety of memristive neural networks in [50–53]. In generic way, memristive terms are used to modulate the local kinetics

^a e-mail: rengd@lut.edu.cn (corresponding author)

of the neural network, that is, each node of the network has one or two memristive terms and the collective spatial patterns are affected by the distribution of initials for the memristive variables. On the other hand, memristive channels are created to control the collective behaviors of the network, which indicates high order coupling [54–58] and field coupling [59–61] are more effective to control the network behaviors effectively.

When memristor is incorporated into an additive branch circuit of the neural circuit, the memristive term accompanying with the magnetic flux variable can describe the effect of electromagnetic induction of neural activities. On the other hand, the memristive coupling channels become controllable under external field energy injection when memristors are used to couple two or more neural circuits. As mentioned above, activation of memristor into the nonlinear circuits can develop complex dynamics and creation of multistability in the memristive systems and networks. Some memristive systems are used for image encryption [62–65]. Indeed, one recent work claimed that a memristor can connect two capacitors for building a memristive cell membrane [66], and this memristive membrane of the biophysical neurons becomes more controllable under energy flow. That is, the physical property of the cell membrane can be discovered from a new aspect, and two capacitive variables are introduced into the neuron model for discerning the effect of membrane flexibility [48, 67, 68]. The electromagnetic induction generated by ion transport inside and outside of the neuron membrane and the influence of external magnetic field on the neuron discharge activity can be explored in a memristor-based nonlinear circuit, and the energy characteristic is discussed for clarifying the self-adaptive property of the memristive neuron.

As is known, Josephson junction can recognize the stimuli from external magnetic field. Therefore, connection of Josephson Junction [42, 43, 69] to a neural circuit can be used to perceive the effect of electromagnetic field on the neural activities. For example, Zhang et al. [70] suggested a Josephson Junction-coupled neural circuit for detecting mode transition under external magnetic field, and then a memristor is connected to the Josephson junction in parallel [71] to improve the sense ability, which inner and outer magnetic field effect can be described synchronously. Besides the model approach and dynamical description, it is more interesting to explore the intrinsic self-adaptive property and energy regulation role during changes of neural activities. In this paper, a memristor-based neuron model is obtained by embedding a MFCM into a simple neuronal circuit. This memristive circuit can estimate the external magnetic field. The energy function for the memristive circuit is defined and then converted into equivalent Hamilton energy function, which can also be confirmed by using the Helmholtz theorem. An adaptive law is suggested to explain the self-adaptive growth and regulation in the memristive channel because of energy injection. Analog circuit is implemented with exact energy estimation.

2 Model and scheme

A memristive neural circuit is developed by connecting a MFCM into the fifth branch of the FHN neural circuit. The memristive channel can keep field energy and its channel current will be changed due to external magnetic field, and the circuit approach is displayed in Fig. 1.

Based on the Kirchhoff’s law, the circuit equations for Fig. 1 can be described by

$$\begin{cases} C \frac{dV}{dt} = \frac{V_s - V}{R_s} - i_L - i_N - i_M; \\ L \frac{di_L}{dt} = V - Ri_L + E. \end{cases} \tag{1}$$

The channel current i_N through the nonlinear resistor R_N in Fig. 1 can be estimated by

$$i_N = -\frac{1}{\rho} \left(V - \frac{1}{3} \frac{V^3}{V_0^2} \right), \tag{2}$$

where ρ and V_0 represent the normalization parameters, and the memristive channel current i_M across the MFCM is given in

$$i_M = M(\varphi)V = \alpha\varphi V, \quad \frac{d\varphi}{dt} = \lambda \tanh(\varphi) - d\varphi + \delta V; \tag{3}$$

Fig. 1 Schematic diagram for single memristive neuron model. V_s denotes an external stimulus source, $M(\varphi)$ is a MFCM, R_s , R and R_N are linear and nonlinear resistors, E , L and C represent constant voltage source, induction coil and capacitor, respectively

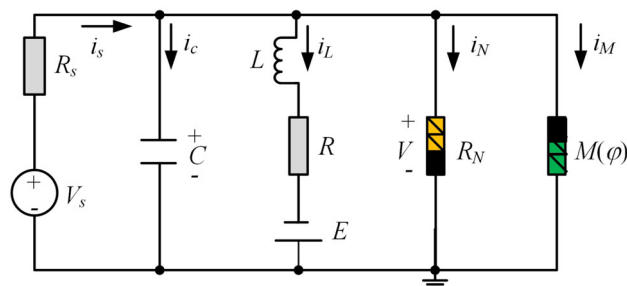
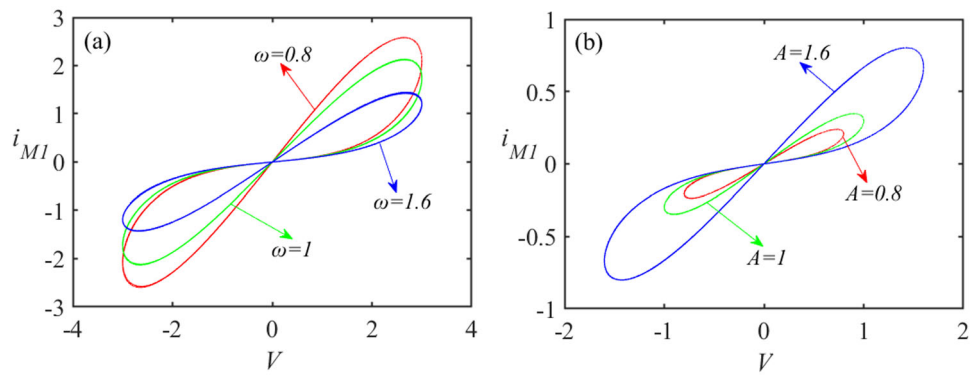


Fig. 2 The $v-i$ curve for MFCM with different stimulus. For **a** $A = 3$; **b** $\omega = 0.8$



where α , δ and d represent the normalization parameters. As shown in Eq. (3), the $M(\varphi)$ has a simple form with low order, and its internal state equation is only composed of linear term. Compared with higher-order memristors, the memristor in this paper is easier to implement physically. By imposing sinusoidal stimulus $A\sin(2\pi\omega t)$, where A means the amplitude of stimulus, ω denotes the frequency of stimulus. The $v-i$ curve for MFCM with different frequencies ω under $A = 3$ is shown in Fig. 2a, the $v-i$ curve for MFCM with different amplitude A with $\omega = 0.8$ is shown in Fig. 2b.

The Fig. 2 show that the $v-i$ curve for MFCM exhibits the characteristic of 8-shaped. The 8-shaped area is decreased when the frequency of stimulus is increased. While the 8-shaped area is increased when the amplitude of stimulus is increased.

The voltage source V_s is selected with periodic form as follows

$$V_s = A_0 \cos(f_0 t). \tag{4}$$

A group of dimensionless variables and parameters are defined by setting scale transformation for the parameters and variables in Eqs. (1)–(4).

$$\begin{cases} x = \frac{V}{V_0}, y = \frac{\rho i_L}{V_0}, z = \frac{\varphi}{\rho C V_0}, \tau = \frac{t}{\rho C}, a = \frac{E}{V_0}, b = \frac{R}{\rho}, c = \frac{\rho^2 C}{L}; \\ \xi = \frac{\rho}{R_s}, A = \frac{\rho A_0}{R_s V_0}, f = \rho C f_0, k = \alpha \rho^2 C V_0, \gamma = d \rho C, \rho = \lambda \rho C. \end{cases} \tag{5}$$

A memristive neuron model is obtained by replacing the variables and parameters in Eq. (1) under the scale criterion in Eq. (5) without external electromagnetic radiation. In presence of external magnetic field, the magnetic flux and channel current across the MFCM will be changed; as a result, the memristive current is modified to regulate the excitability and firing modes of the neuron. Therefore, external disturbance term is added to regulate the right side of the formula for magnetic flux variable shown in Eq. (7).

$$\begin{cases} \frac{dx}{d\tau} = x(1 - \xi) - \frac{1}{3}x^3 - y - kzx + A \cos(f\tau); \\ \frac{dy}{d\tau} = c(x - by + a); \\ \frac{dz}{d\tau} = \rho \tanh(z) - \gamma z + \delta x; \end{cases} \tag{6}$$

Both the memristive current (induction current) kzx and the external stimulus $A\cos(f\tau)$ have impacts on the excitability, and any changes of the two kinds of currents will modify the firing patterns of the neuron. External magnetic field has an impact on the inner magnetic field of the memristor, and then channel current is changed by introducing additive disturbance φ_{ext} on the third variable for magnetic flux as follows

$$\begin{cases} \frac{dx}{d\tau} = x(1 - \xi) - \frac{1}{3}x^3 - y - kzx + A \cos(f\tau); \\ \frac{dy}{d\tau} = c(x - by + a); \\ \frac{dz}{d\tau} = \rho \tanh(z) - \gamma z + \delta x + \varphi_{ext}, \end{cases} \tag{7}$$

where φ_{ext} denotes an external magnetic field, here, φ_{ext} can be considered as a constant for a static magnetic field or a periodic form for a changeable magnetic field, respectively. Furthermore, the physical field energy in the memristive neural circuit in Fig. 1 is calculated by

$$W = W_C + W_L + W_M = \frac{1}{2}CV^2 + \frac{1}{2}Li_L^2 + \frac{1}{2}\varphi i_M. \tag{8}$$

By applying the same scale transformation in Eq. (5) on the field energy in Eq. (8), the Hamilton energy function in dimensionless form is obtained by

$$H = H_C + H_L + H_M = \frac{W}{CV_0^2} = \frac{W_C}{CV_0^2} + \frac{W_L}{CV_0^2} + \frac{W_M}{CV_0^2} = \frac{1}{2}x^2 + \frac{1}{2c}y^2 + \frac{1}{2}kz^2x. \tag{9}$$

According to the Eq. (9), the Hamilton energy function of an isolated memristive neuron mainly depends on the variables (x, y, z) and two normalized parameters (c, k). The Hamilton energy function for the memristive neuron in Eq. (6) can also be approached in a theoretical way, based on the Helmholtz theorem, the memristive neuron is written in equivalent vector form in Eqs. (10a, 10b).

$$\begin{aligned} \begin{pmatrix} \dot{x} \\ \dot{y} \\ \dot{z} \end{pmatrix} &= \begin{pmatrix} x(1 - \xi) - 1/3x^3 - y - kzx + A \cos(f\tau) \\ c(x + a - by) \\ \rho \tanh(z) - \gamma z + \delta x \end{pmatrix} = F_c + F_d \\ &= \begin{pmatrix} -y - \delta kzx \\ cx + 0.5ckz^2 \\ \delta x + 0.5\delta kz^2 \end{pmatrix} + \begin{pmatrix} x(1 - \xi) - 1/3x^3 + A \cos(f\tau) - (1 - \delta)kzx \\ c(a - by) - 0.5ckz^2 \\ \rho \tanh(z) - \gamma z - 0.5\delta kz^2 \end{pmatrix} \\ &= \begin{pmatrix} 0 & -c & -\delta \\ c & 0 & 0 \\ \delta & 0 & 0 \end{pmatrix} \begin{pmatrix} x + 0.5kz^2 \\ y \\ c \\ kzx \end{pmatrix} + \begin{pmatrix} A_{11} & 0 & 0 \\ 0 & A_{22} & 0 \\ 0 & 0 & A_{33} \end{pmatrix} \begin{pmatrix} x + 0.5kz^2 \\ y \\ c \\ kzx \end{pmatrix}. \end{aligned} \tag{10a}$$

$$\begin{aligned} A_{11} &= \frac{x(1 - \xi) - 1/3x^3 + A \cos(f\tau) - (1 - \delta)kzx}{x + 0.5kz^2}; \\ A_{22} &= \frac{c(c(a - by) - 0.5ckz^2)}{y}; \\ A_{33} &= \frac{\rho \tanh(z) - \gamma z - 0.5\delta kz^2}{kzx}. \end{aligned} \tag{10b}$$

The Hamilton energy function H meets the following criterion according to the Helmholtz theorem

$$\nabla H^T F_c = 0; \quad \nabla H^T F_d = \dot{H} = \frac{dH}{d\tau}. \tag{11}$$

A sole Hamilton energy function can be exact solution for the formula as follows

$$0 = \nabla H^T F_c = (-y - \delta kzx) \frac{\partial H}{\partial x} + \frac{y}{c} \frac{\partial H}{\partial y} + (\delta x + 0.5\delta kz^2) \frac{\partial H}{\partial z}; \tag{12}$$

Indeed, an exact solution for Eq. (12) can be obtained to be identical to the Hamilton energy function in Eq. (9)

$$H = \frac{1}{2}x^2 + \frac{1}{2c}y^2 + \frac{1}{2}kz^2x; \tag{13}$$

That is, the memristive neuron holds exact energy function and the energy can be shunted from the memristive channel considered as energy source ($H_M = 0.5kxz^2 < 0$). The first two terms in Eq. (13) always keep positive value, the third term can become negative value, it indicates the memristive channel can release energy and external energy source can be captured.

3 Results and discussions

In this section, the numerical solutions for a single memristive neuron are obtained on the MATLAB platform by applying the four-order Runge–Kutta algorithm with time step $h = 0.01$. The parameters of the neuron model are selected as $a = 0.7, b = 0.8, c = 0.1, \xi = 0.25, k = 0.01, \rho = 0.01, \delta = 0.1, \gamma = 0.1$. In Fig. 3, the bifurcation analysis and the largest Lyapunov exponent (LLE) for the memristive neuron are calculated by varying the periodic voltage source.

The results in Fig. 3 show that the memristive neuron can be induced to present bursting, spiking and chaotic firing patterns by adjusting the frequency of external stimulus. In fact, the firing patterns for the memristive neuron can be controlled by applying the periodic voltage source. Furthermore, firing patterns and the changes of Hamilton energy for the memristive neuron are shown in Fig. 4 by changing the frequency for the voltage source.

Figure 4 illustrates that the memristive neuron can be excited to show three kinds of firing modes during taming the frequency for external stimulus, and the memristive neuron has higher mean value of Hamilton energy with bursting and spiking firing patterns, while it has lower mean value of Hamilton energy accompanying with chaotic modes.

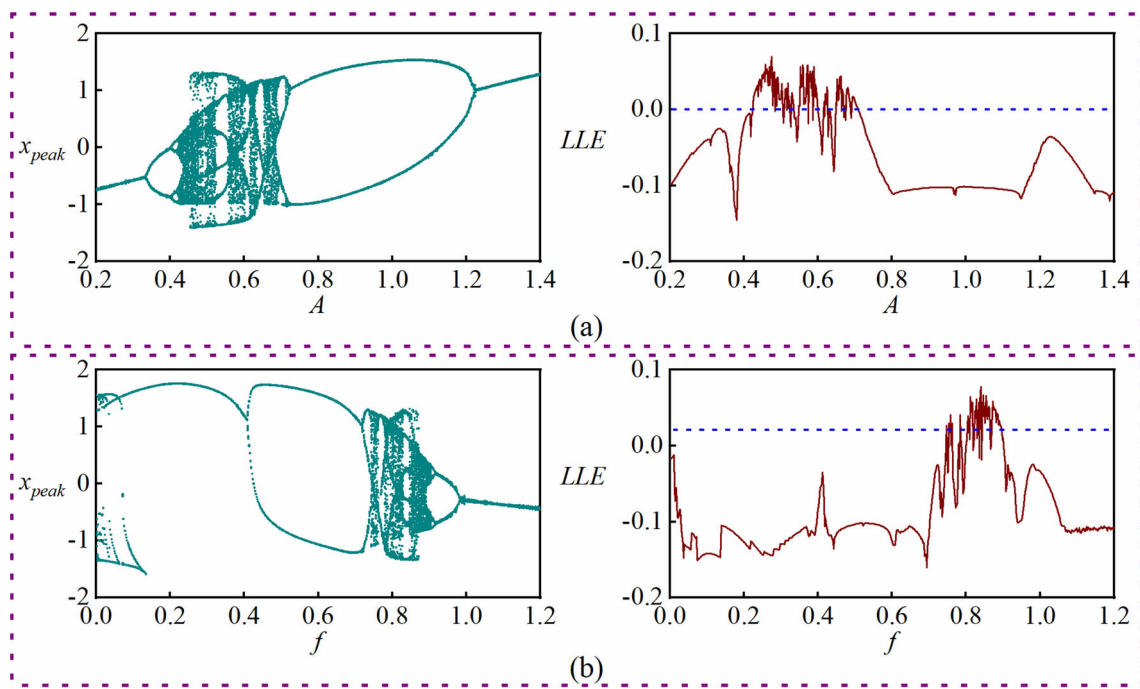
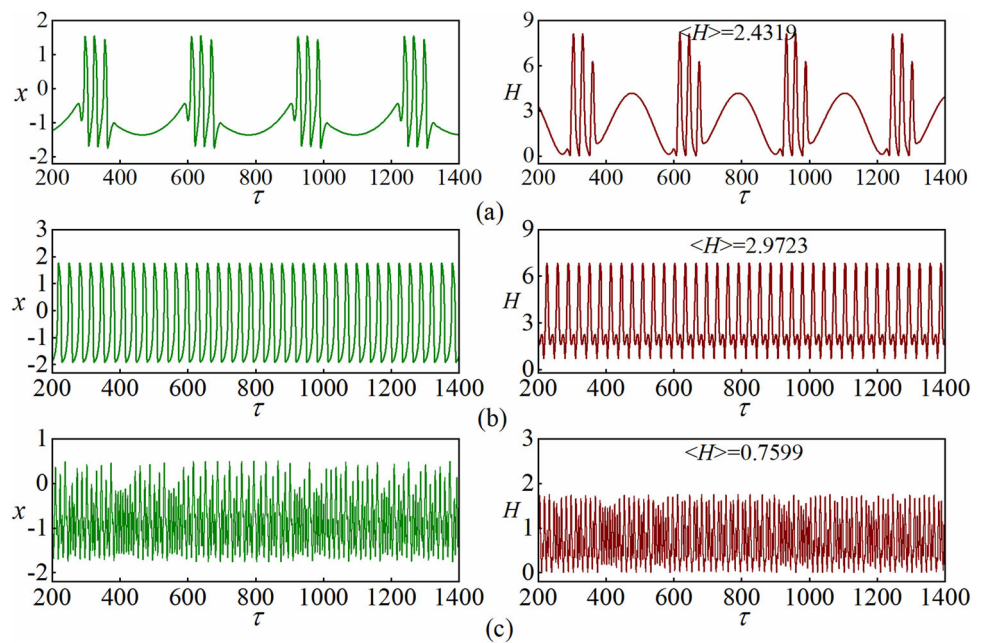


Fig. 3 Bifurcation diagram and *LLE* for the neuron driven by the periodic voltage source. For **a** $f = 0.8$; **b** $A = 0.6$. Parameters are chosen as $a = 0.7, b = 0.8, c = 0.1, \xi = 0.25, k = 0.01, \rho = 0.01, \delta = 0.1, \gamma = 0.1$, and initial value is set as $(0.2, 0.1, 0.01)$. x_{peak} denotes peak values of membrane potential

Fig. 4 Sampled time series of membrane potential and evolution of Hamilton energy with different f . For **a** $f = 0.02$; **b** $f = 0.2$; **c** $f = 0.88$. Parameters are chosen as $a = 0.7, b = 0.8, c = 0.1, \xi = 0.25, k = 0.01, \rho = 0.01, \delta = 0.1, \gamma = 0.1, A = 0.6$, and initials $(0.2, 0.1, 0.01)$. $\langle H \rangle$ denotes the mean value of Hamilton energy



As shown in Eq. (7), the neuron is placed into a stable magnetic field when φ_{ext} is considered as a constant signal φ_c . Changing the intensity of external magnetic field, magnetic flux is regulated synchronously and the results are plotted in Fig. 5 by calculating the distribution of *LLE* for the memristive neuron under setting different values for φ_c .

It is confirmed that a memristive neuron exhibits periodic and chaotic firing modes when an external magnetic field is applied with suitable intensity. Additionally, the memristive neuron undergoes mode transition from a periodic state to a chaotic state through reverse period-doubling bifurcation when the external magnetic field increases from 0 to 1. That is, the strength of the external magnetic field controls the complex firing activities of memristor neurons such as periodic, chaotic patterns. The evolution of membrane potential and changes of Hamilton energy corresponding to periodic and chaotic modes are shown in Fig. 6.

The results in Fig. 6 show that periodic firing mode has a higher average value of the Hamilton energy, while chaotic pattern has a lower mean value of the Hamilton energy. Furthermore, the effect of periodic magnetic field on the electrical activity of neuron is

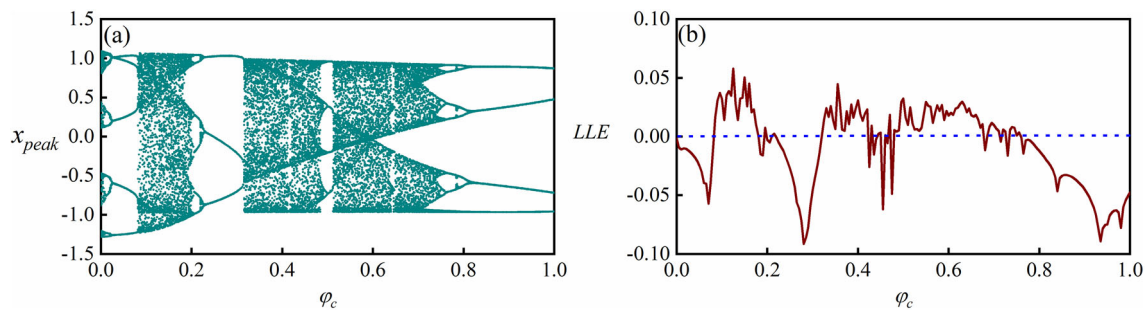


Fig. 5 Bifurcation diagram and *LLE* for the neuron under constant magnetic field φ_c . For **a** bifurcation diagram; **b** *LLE*. Parameters are chosen as $a = 0.7$, $b = 0.8$, $c = 0.1$, $\xi = 0.25$, $k = 0.01$, $\rho = 0.01$, $\delta = 0.1$, $\gamma = 0.1$, $A = 0.6$, $f = 0.8$, and initials (0.2, 0.1, 0.01)

Fig. 6 Sampled time series of membrane potential and evolution of Hamilton energy with different external magnetic field φ_c . For **a** $\varphi_c = 0.3$; **b** $\varphi_c = 0.6$. Parameters are chosen as $a = 0.7$, $b = 0.8$, $c = 0.1$, $\xi = 0.25$, $k = 0.01$, $\rho = 0.01$, $\delta = 0.1$, $\gamma = 0.1$, $A = 0.6$, $f = 0.8$, and initials (0.2, 0.1, 0.01). $\langle H \rangle$ denotes the mean value of Hamilton energy

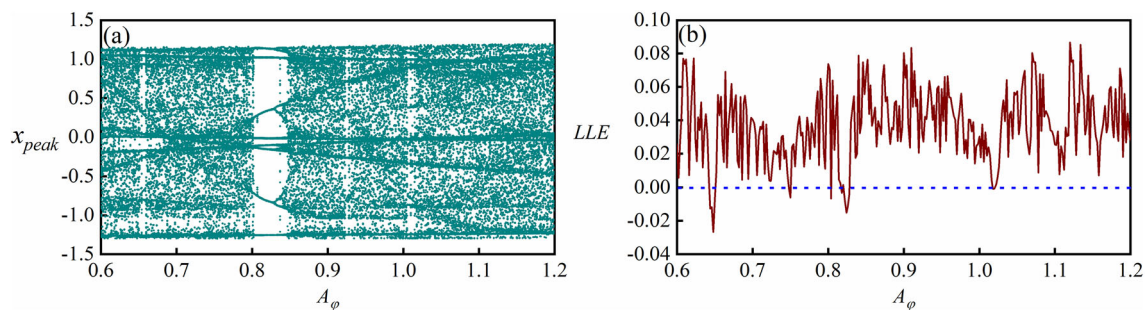
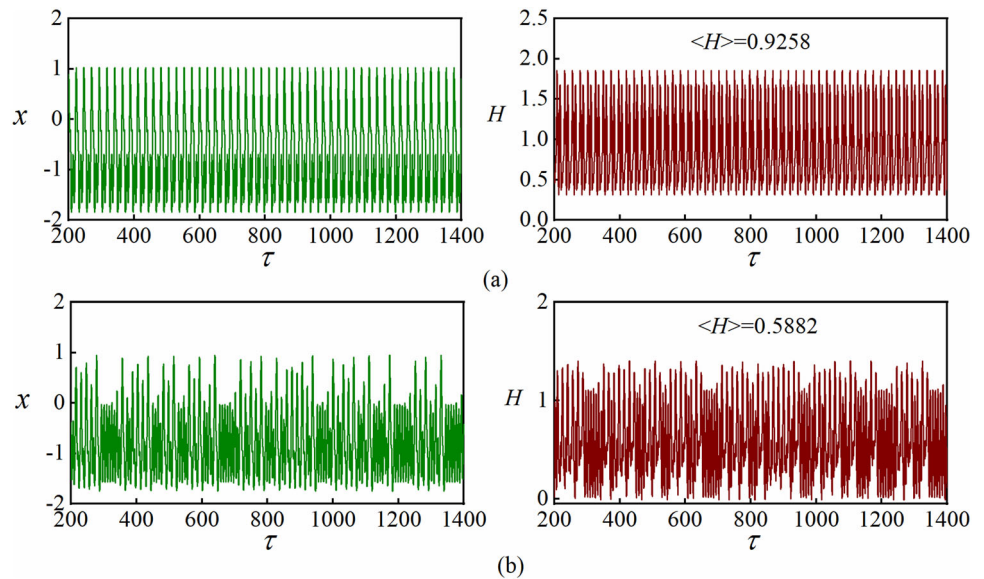


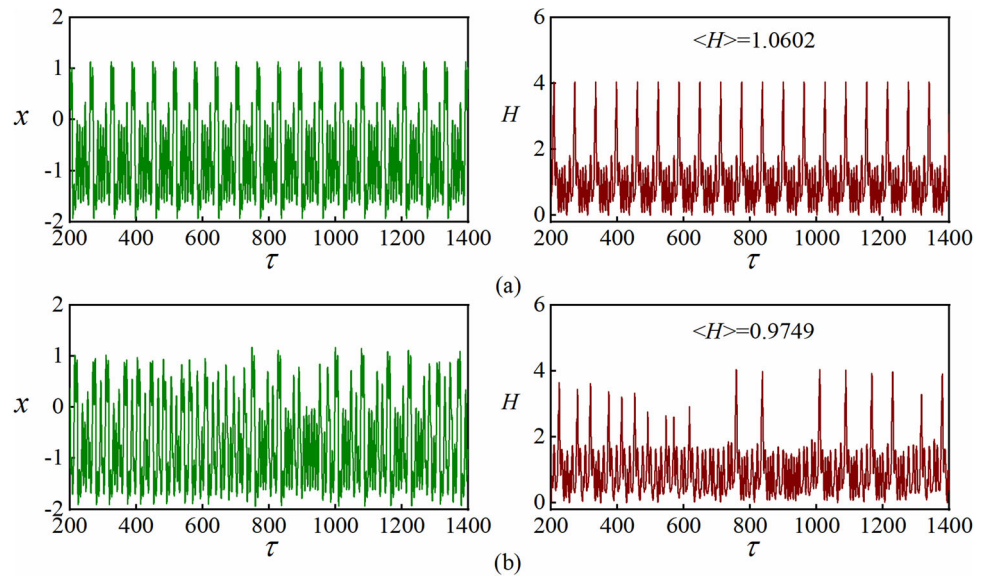
Fig. 7 Bifurcation diagram and *LLE* for the neuron by changing the amplitude A_φ for external magnetic field. For **a** bifurcation diagram; **b** *LLE*. Parameters are chosen as $a = 0.7$, $b = 0.8$, $c = 0.1$, $\xi = 0.25$, $k = 0.01$, $\rho = 0.01$, $\delta = 0.1$, $\gamma = 0.1$, $A = 0.6$, $f = 0.8$, $f_\varphi = 0.4$, and initials (0.2, 0.1, 0.01)

discussed. The time-varying external magnetic field is considered as $\varphi_{ext} = A_\varphi \sin f_\varphi \tau$, here, A_φ denotes the amplitude and f_φ is the frequency of a periodic external magnetic field. The parameters and initial values are kept as above, f_φ is fixed at 0.4, the bifurcation diagram and LLE are calculated by changing the value for A_φ , and the results are plotted in Fig. 7.

The results in Fig. 7 indicate that there are four periodic windows are occurred in the range of amplitude a from 0.6 to 1.2, and the chaotic modes are distributed in a large parameter range. Similar to the case of constant external magnetic field, the firing mode of memristor neurons is completely controlled by periodic external magnetic field. Furthermore, the relation between firing patterns and the Hamilton energy is calculated by selecting different values A_φ , and evolution of membrane potential accompanying with energy changes are displayed in Fig. 8.

Similar to the results in Fig. 6, the periodic state exhibits a higher average Hamilton energy value, while the chaotic modes occur a lower average Hamilton energy value. In fact, the applied external magnetic field just injected energy flow into the media and the neural circuit, and the captured energy will be propagated and shared between the capacitive and inductive channels including the

Fig. 8 Evolution of membrane potential and Hamilton energy for the neuron under periodic external magnetic field. For **a** $A_\varphi = 0.82$; **b** $A_\varphi = 0.92$. Parameters are chosen as $a = 0.7, b = 0.8, c = 0.1, \xi = 0.25, k = 0.01, \rho = 0.01, \delta = 0.1, \gamma = 0.1, A = 0.6, f = 0.8, f_\varphi = 0.4$, and initial value is set as $(0.2, 0.1, 0.01)$. $\langle H \rangle$ denotes the mean value of Hamilton energy



capacitor channel, the induction coil channel and the memristor channel. Any changes of energy proportion between these channels and electric components will modify the excitability, and the firing modes are changed even accompanying with parameter shift because of shape deformation in some electric components. To explore the adaptability of the memristor channel in memristive neurons, energy flow is used to control the adaptive growth of the memristor channel. That is, the energy ratio between capacitive and inductive channels will predict possible mode transition, and shape deformation of memristive channels due to large energy injection can be approached by using adaptive parameter shift as follows

$$\frac{dk}{d\tau} = \kappa \cdot k \cdot \theta\left(\varepsilon - \left|\frac{H_M}{H_L}\right|\right), \quad \theta(p) = 1, \quad p \geq 0, \quad \theta(p) = 0, \quad p < 0; \tag{14}$$

where gain κ controls the growth of the parameter k for the memristive current, the threshold $0 < \varepsilon < 1$ determines the energy ratio of a memristive channel to inductive channel energy in the neuron. At first, the case of a constant external magnetic field is discussed. Parameters are selected as $a = 0.7, b = 0.8, c = 0.1, \xi = 0.25, \rho = 0.01, \delta = 0.1, \gamma = 0.1, A = 0.6, f = 0.8$, and the initial values for variables are set as $(0.2, 0.1, 0.01)$. The initial value of parameter k is fixed at 0.001, threshold for ε is fixed as 0.4, and a constant external magnetic field is given as $\varphi_c = 0.1$. The adaptive growth of k , membrane potential and Hamilton energy for different parameter κ are calculated, the results are shown in Fig. 9.

It is found that the parameter k reaches a stable value (1.54) after a transient period (867 time unites). The membrane potential and Hamilton energy also maintain periodic oscillations with time. By setting larger value for the gain κ , k reaches a stable value in a smaller transient period. Chaos theory often emphasizes sensitivity to initial conditions as a defining characteristic. To explore the sensitivity of the memristive system to initial values, the time sampling sequence of the membrane potential with different initial values are calculated, and the results are shown in Fig. 10.

The results in Fig. 10 illustrate that this memristive neuron model is highly sensitive to initial values. The circuit simulation of the memristive neuron can be realized by applying the Multisim software. The neuron model presented in Eq. (6) is transformed on a time scale by applying $\tau = 100t$, and the Eq. (6) is updated as follows

$$\begin{cases} \frac{dx}{dt} = 100x(1 - \xi) - \frac{100}{3}x^3 - 100y - 100kzx + 100A \cos(100f\tau); \\ \frac{dy}{dt} = 100cx - 100by + 100a; \\ \frac{dz}{dt} = 100\rho \tanh(z) - 100\gamma z + 100\delta x; \end{cases} \tag{15}$$

Parameters are chosen as $a = 0.7, b = 0.8, c = 0.1, \xi = 0.25, k = 0.01, \rho = 0.01, \delta = 0.1, \gamma = 0.1, A = 0.6$, and initial value is set as $(0.2, 0.1, 0.01)$. The corresponding analog circuit is shown in Fig. 11.

According to Fig. 11, the state equations can be described by

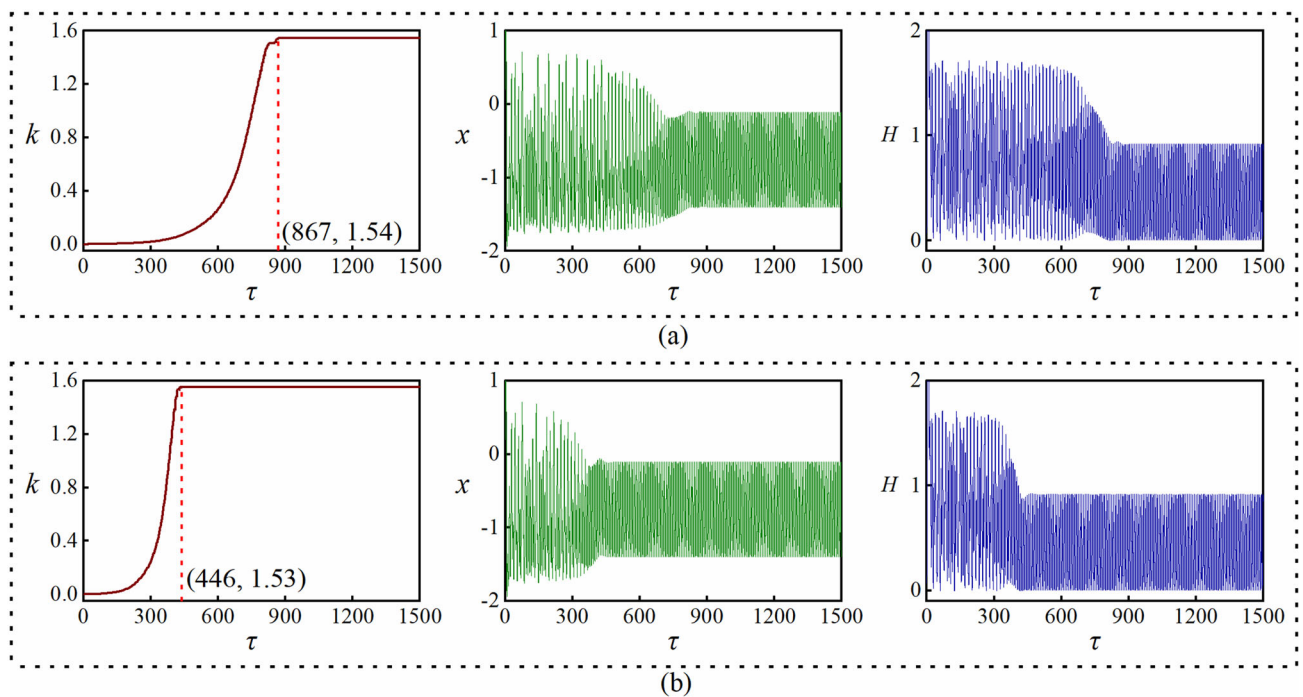


Fig. 9 The growth of k , membrane potential and Hamilton energy. For **a** $\kappa = 0.01$; **b** $\kappa = 0.02$

Fig. 10 Sampled time series of membrane potential with different initial values. For **a** $(0.2 + 10^{-15}, 0.1, 0.01)$, $(0.2, 0.1, 0.01)$; **b** $(0.2, 0.1 + 10^{-15}, 0.01)$, $(0.2, 0.1, 0.01)$. Parameters are chosen as $a = 0.7$, $b = 0.8$, $c = 0.1$, $\xi = 0.25$, $k = 0.01$, $\rho = 0.01$, $\delta = 0.1$, $\gamma = 0.1$, $A = 0.6$, $f = 0.88$

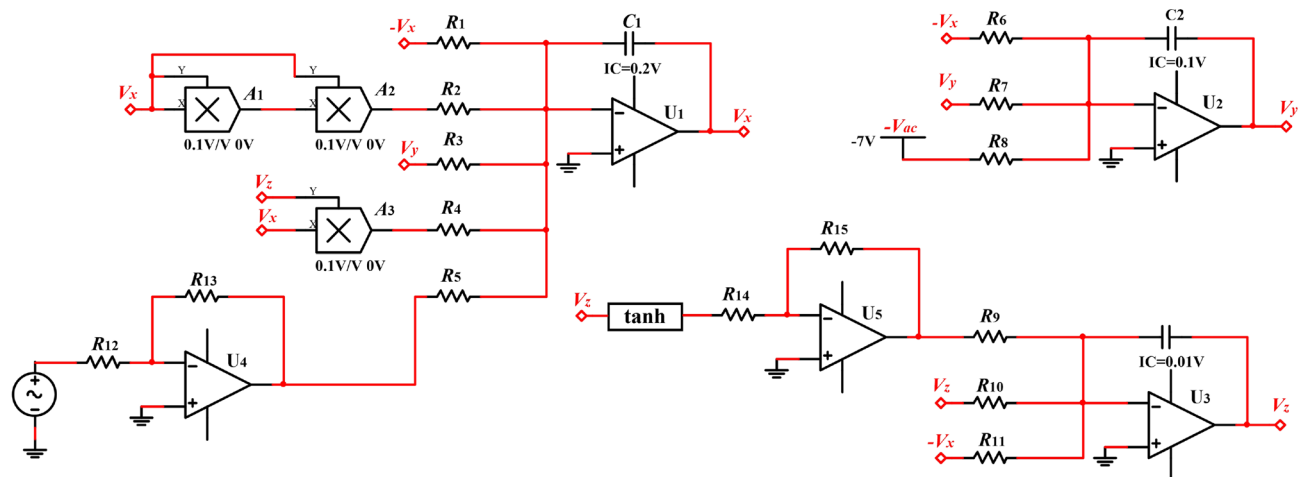
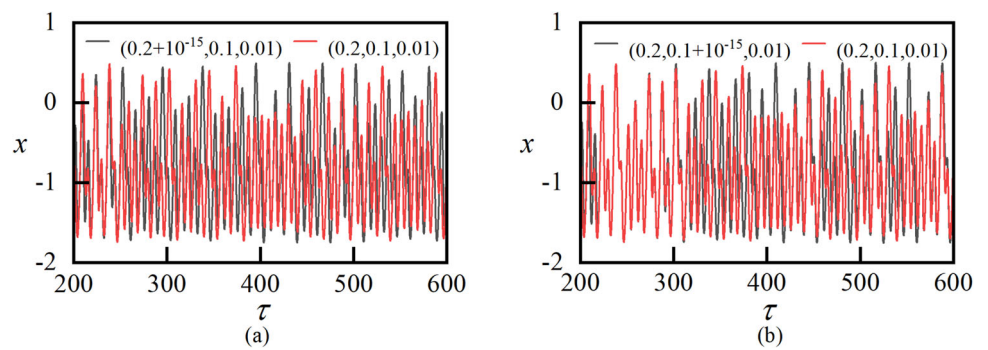
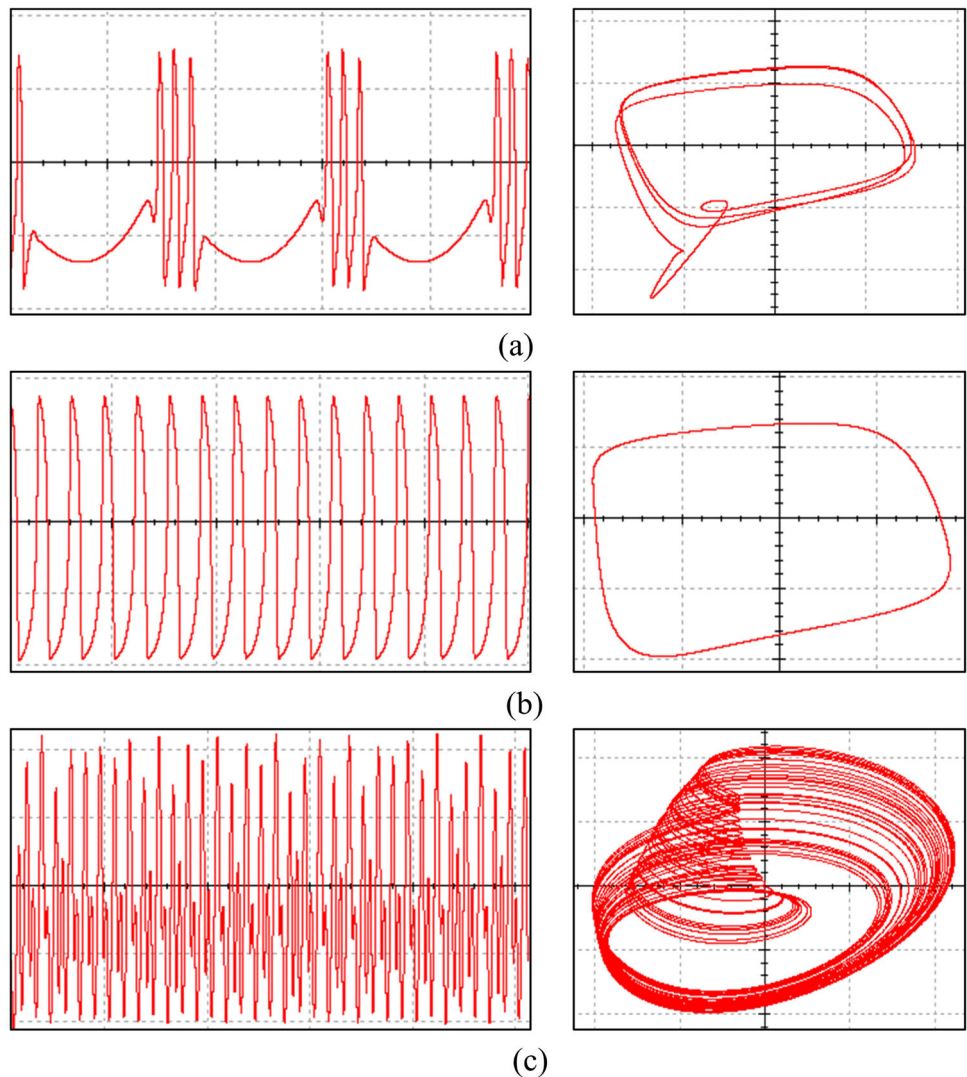


Fig. 11 The analog circuit of the memristive neuron

Fig. 12 Output voltages and formed attractors on the Multisim platform. For **a** membrane potential and phase diagram for $f = 0.318$; **b** membrane potential and phase diagram for $f = 3.18$; **c** membrane potential and phase diagram for $f = 14.005$



$$\begin{cases} C_1 \frac{dV_x}{dt} = \frac{1}{R_1} V_x - \frac{1}{100R_2} V_x^3 - \frac{1}{R_3} V_y - \frac{1}{10R_4} V_z V_x + \frac{1}{R_5} A \cos(2\pi ft); \\ C_2 \frac{dV_y}{dt} = \frac{1}{R_6} V_x - \frac{1}{R_7} V_y + \frac{1}{R_8} V_{ac}; \\ C_3 \frac{dV_z}{dt} = \frac{1}{R_9} \tanh(V_z) - \frac{1}{R_{10}} V_z + \frac{1}{R_{11}} V_x; \end{cases} \tag{16}$$

In addition, the energy for the neural circuit is mainly kept in capacitive form as follows

$$W = \frac{1}{2} C_1 V_x^2 + \frac{1}{2} C_2 V_y^2 + \frac{1}{2} C_3 V_z^2. \tag{17}$$

In Fig. 11, the capacitance and resistance parameters are fixed as $C_1 = C_2 = C_3 = 10 \text{ nF}$, $R_1 = 1333.3 \text{ k}\Omega$, $R_2 = 30 \text{ k}\Omega$, $R_3 = R_5 = 1000 \text{ k}\Omega$, $R_4 = R_6 = R_{10} = R_{11} = 10,000 \text{ k}\Omega$, $R_8 = R_9 = 100,000 \text{ k}\Omega$, $R_{12} = R_{13} = R_{14} = R_{15} = 10 \text{ k}\Omega$, and Multiplier is $A_1 = A_2 = A_3 = 0.1$. The simulation results by applying the oscilloscopes on the Multisim software are displayed in Fig. 12.

The results in Fig. 12 confirmed that the memristive neuron can be realized by analog circuits, which will provide a good theoretical basis and experimental guidance for the application of neuron model driven mechanism. Furthermore, according to energy function presented in Eq. (17), the analog circuit for energy function is shown in Fig. 13.

The state equation for energy in Fig. 11 can be expressed by

$$W = \frac{R_{16}}{R_{17}} V_x^2 + \frac{R_{16}}{R_{18}} V_y^2 + \frac{R_{16}}{R_{19}} V_z^2; \tag{18}$$

Fig. 13 The analog circuit of the memristive neuron

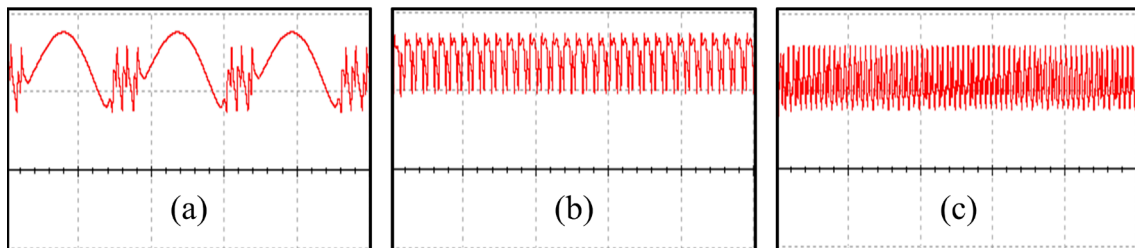
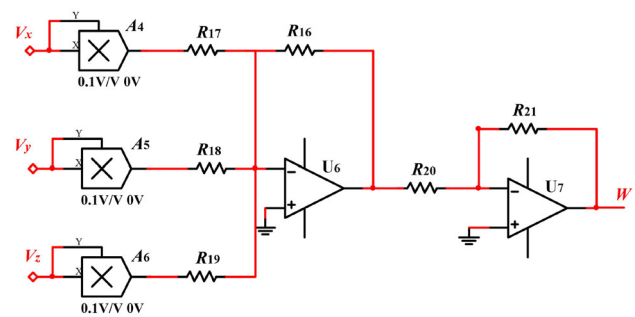


Fig. 14 Simulation results for energy on the Multisim platform. For **a** bursting firing; **b** spiking firing; **c** chaotic firing

In Fig. 13, the resistance parameters are fixed as $R_{16} = 50 \Omega$, $R_{17} = R_{18} = R_{19} = 100,000 k\Omega$, $R_{20} = R_{21} = 10 k\Omega$, and Multiplier is $A_4 = A_5 = A_6 = 0.1$. Based on the analog circuits in Figs. 11, 13, The energy sequences corresponding to the firing modes in Fig. 13 are displayed in Fig. 14. Due to the small value of W , the results in Fig. 14 are magnified by a factor of 10 in order to observe the output sequence of W significantly in the oscilloscope.

The results indicate that the energy function is dependent on the firing mode, and analog circuit approach is consistent with the results of numerical approach of the memristive neuron model.

In summary, an involvement of memristor into simple FHN neural circuit is effective to detect and describe the effect of external magnetic field on the neural activities. The energy level accounts for mode selection and then external stimuli including electromagnetic radiation can inject energy into the media, as a result, the firing activities of the neuron can be controlled completely. In fact, noisy disturbance on the membrane potential or the magnetic flux due to electromagnetic radiation can be imposed on this memristive neuron, similar coherence resonance and stochastic resonance can be induced, and the curve for SNR (signal to noise ratio) and average Hamilton energy will provide fast way of this prediction. From physical aspect, large energy injection can cause some shape deformation of the electric components even damage, therefore, one or more intrinsic parameters of these electric components will be changed under energy flow. As a result, fast and effective energy shunting and exchange between different channels and components are crucial for keeping safe running of these neural circuits, and the biophysical neurons release their self-adaptive property by adjusting the intrinsic parameters in adaptive way.

4 Conclusion

A memristive neural circuit sensitive to the magnetic field is proposed. According to the famous Helmholtz theorem, the Hamilton energy for the memristive neuron is approached in theoretical way, and it is also confirmed by applying scale transformation on the field energy for the neural circuit. The electrical activities and field energy distribution of the memristive neuron under the different types of the magnetic field are investigated in detail. The numerical results show that neuron can be controlled to present suitable firing patterns, in particular, continuous mode transition occurs under the self-adaptive law, which one intrinsic parameter of memristive synapse controls its growth under the energy flow. The potential mechanism is that energy accumulation and external energy injection induce shape deformation of the memristive channels, and one parameter is changed to keep safe energy level in this memristor. It prefers to keep periodic firing patterns when the average field energy maintains a higher level. The memristive neuron can be realized by applying analog circuit on the Multisim platform.

Acknowledgements This project is supported by the National Natural Science Foundation of China under Grant No. 12072139.

Author contribution Feifei Yang finished model approach and numerical solution, Zhitang Han verified circuit tests, Guodong Ren polished the draft and proof checking, circuit verification. Qun Guo and Jun Ma edited the writing and formal analysis, and the projection suggested by Jun Ma.

Data availability The data used to support the findings of this study are available from the corresponding author upon request. The manuscript has associated data in a data repository.

Declarations

Conflict of interest The authors declare that they have no conflict of interest.

References

1. L. Chua, Memristor-the missing circuit element. *IEEE Trans. Circuit Theory* **18**, 507–519 (1971)
2. A. Isah, A.S.T. Nguetcho, S. Binczak et al., Dynamics of a charge-controlled memristor in master-slave coupling. *Electron. Lett.* **56**, 211–213 (2020)
3. K.J. Chandía, M. Bologna, B. Tellini, Multiple scale approach to dynamics of an LC circuit with a charge-controlled memristor. *IEEE Trans. Circuits Syst. II Express Br.* **65**, 120–124 (2017)
4. Z.Q. Chen, H. Tang, Z.L. Wang et al., Design and circuit implementation for a novel charge-controlled chaotic memristor system. *J. Appl. Anal. Comput.* **5**, 251–261 (2015)
5. C. Li, Y. Yang, J. Du et al., A simple chaotic circuit with magnetic flux-controlled memristor. *Eur. Phys. J. Spec. Top.* **230**, 1723–1736 (2021)
6. D. Batas, H. Fiedler, A memristor SPICE implementation and a new approach for magnetic flux-controlled memristor modeling. *IEEE Trans. Nanotechnol.* **10**, 250–255 (2010)
7. C. Wang, L. Zhou, R. Wu, The design and realization of a hyper-chaotic circuit based on a flux-controlled memristor with linear memductance. *J. Circuits, Syst. Comput.* **27**, 1850038 (2018)
8. Y. Chen, J. Mou, H. Jahanshahi et al., A new mix chaotic circuit based on memristor–memcapacitor. *Eur. Phys. J. Plus* **138**, 78 (2023)
9. J. Luo, W. Tang, Y. Chen et al., Dynamical analysis and synchronization control of flux-controlled memristive chaotic circuits and its FPGA-based implementation. *Results Phys.* **54**, 107085 (2023)
10. G. Peng, F. Min, Multistability analysis, circuit implementations and application in image encryption of a novel memristive chaotic circuit. *Nonlinear Dyn.* **90**, 1607–1625 (2017)
11. N. Wang, G. Zhang, H. Bao, Bursting oscillations and coexisting attractors in a simple memristor-capacitor-based chaotic circuit. *Nonlinear Dyn.* **97**, 1477–1494 (2019)
12. X. Ye, J. Mou, C. Luo et al., Dynamics analysis of Wien-bridge hyperchaotic memristive circuit system. *Nonlinear Dyn.* **92**, 923–933 (2018)
13. B. Bao, Q. Zhao, X. Yu et al., Complex dynamics and initial state effects in a two-dimensional sine-bounded memristive map. *Chaos Solitons Fractals* **173**, 113748 (2023)
14. Y.G. Yang, F.E. Cheng, D.H. Jiang et al., A visually meaningful image encryption algorithm based on P-tensor product compressive sensing and newly-designed 2D memristive chaotic map. *Phys. Scr.* **98**, 105211 (2023)
15. Y. Li, C. Li, Q. Zhong et al., A memristive chaotic map with only one bifurcation parameter. *Nonlinear Dyn.* **112**, 3869–3886 (2024)
16. S. Zhang, H. Zhang, C. Wang, Dynamical analysis and applications of a novel 2-D hybrid dual-memristor hyperchaotic map with complexity enhancement. *Nonlinear Dyn.* **111**, 15487–15513 (2023)
17. H. Li, Z. Hua, H. Bao et al., Two-dimensional memristive hyperchaotic maps and application in secure communication. *IEEE Trans. Industr. Electron.* **68**, 9931–9940 (2020)
18. Y. Deng, Y. Li, Bifurcation and bursting oscillations in 2D non-autonomous discrete memristor-based hyperchaotic map. *Chaos Solitons Fractals* **150**, 111064 (2021)
19. L. Huang, J. Liu, J. Xiang et al., Design and analysis of a three-dimensional discrete memristive chaotic map with infinitely wide parameter range. *Phys. Scr.* **97**, 065210 (2022)
20. R. Wang, C. Li, S. Kong et al., A 3D memristive chaotic system with conditional symmetry. *Chaos Solitons Fractals* **158**, 111992 (2022)
21. Z. Fan, C. Zhang, Y. Wang et al., Construction, dynamic analysis and DSP implementation of a novel 3D discrete memristive hyperchaotic map. *Chaos Solitons Fractals* **177**, 114303 (2023)
22. B. Xu, X. She, L. Jiang et al., A 3D discrete memristor hyperchaotic map with application in dual-channel random signal generator. *Chaos Solitons Fractals* **173**, 113661 (2023)
23. Q. Lai, L. Yang, A new 3-D memristive hyperchaotic map with multi-parameter-relied dynamics. *IEEE Trans. Circuits Syst. II Express Br.* **70**, 1625–1629 (2022)
24. M. Wang, L. Tong, C. Li et al., A novel four-dimensional memristive hyperchaotic map based on a three-dimensional parabolic chaotic map with a discrete memristor. *Symmetry* **2023**, 15 (1879)
25. Y. Peng, S. He, K. Sun, A higher dimensional chaotic map with discrete memristor. *AEU-Int. J. Electron. Commun.* **129**, 153539 (2021)
26. B. Ramakrishnan, M. Mehrabbeik, F. Parastesh et al., A new memristive neuron map model and its network's dynamics under electrochemical coupling. *Electronics* **11**, 153 (2022)
27. Q. Xu, L. Huang, N. Wang et al., Initial-offset-boosted coexisting hyperchaos in a 2D memristive Chialvo neuron map and its application in image encryption. *Nonlinear Dyn.* **111**, 20447–20463 (2023)
28. H. Bao, K.X. Li, J. Ma et al., Memristive effects on an improved discrete Rulkov neuron model. *Sci China Technol. Sci.* **66**, 3153–3163 (2023)
29. H. Cao, Y. Wang, S. Banerjee et al., A discrete Chialvo–Rulkov neuron network coupled with a novel memristor model: design, dynamical analysis, DSP implementation and its application. *Chaos Solitons Fractals* **179**, 114466 (2024)
30. M. Wang, J. Mou, L. Qin et al., A memristor-coupled heterogeneous discrete neural networks with infinite multi-structure hyperchaotic attractors. *Eur. Phys. J. Plus* **138**, 1137 (2023)
31. P. Lin, C. Li, Z. Wang et al., Three-dimensional memristor circuits as complex neural networks. *Nat. Electron.* **3**, 225–232 (2020)
32. M. Hu, C.E. Graves, C. Li et al., Memristor-based analog computation and neural network classification with a dot product engine. *Adv. Mater.* **30**, 1705914 (2018)
33. F. Yang, J. Ma, Creation of memristive synapse connection to neurons for keeping energy balance. *Pramana* **97**, 55 (2023)
34. Y. Guo, Z. Zhu, C. Wang et al., Coupling synchronization between photoelectric neurons by using memristive synapse. *Optik* **218**, 164993 (2020)
35. F. Wu, Y. Guo, J. Ma, Reproduce the biophysical function of chemical synapse by using a memristive synapse. *Nonlinear Dyn.* **109**, 2063–2084 (2022)
36. B. Hou, X. Hu, Y. Guo et al., Energy flow and stochastic resonance in a memristive neuron. *Phys. Scr.* **98**, 105236 (2023)
37. F. Yang, Y. Xu, J. Ma, A memristive neuron and its adaptability to external electric field. *Chaos: Interdiscipl. J. Nonlinear Sci.* **33**, 023110 (2023)

38. F. Yang, G. Ren, J. Tang, Dynamics in a memristive neuron under an electromagnetic field. *Nonlinear Dyn.* **111**, 21917–21939 (2023)
39. F.Q. Wu, Y.T. Guo, J. Ma, Energy flow accounts for the adaptive property of functional synapses. *Sci. China Technol. Sci.* **66**, 3139–3152 (2023)
40. F. Wu, H. Meng, J. Ma, Reproduced neuron-like excitability and bursting synchronization of memristive Josephson junctions loaded inductor. *Neural Netw.* **169**, 607–621 (2024)
41. F. Wu, Y. Guo, J. Ma et al., Synchronization of bursting memristive Josephson junctions via resistive and magnetic coupling. *Appl. Math. Comput.* **455**, 128131 (2023)
42. A. Mishra, S. Ghosh, S. Kumar Dana et al., Neuron-like spiking and bursting in Josephson junctions: a review. *Chaos: Interdiscipl. J. Nonlinear Sci.* **31**, 052101 (2021)
43. F. Wu, Z. Yao, Dynamics of neuron-like excitable Josephson junctions coupled by a metal oxide memristive synapse. *Nonlinear Dyn.* **111**, 13481–13497 (2023)
44. Z.T. Njitacke, B. Ramakrishnan, K. Rajagopal et al., Extremely rich dynamics of coupled heterogeneous neurons through a Josephson junction synapse. *Chaos Solitons Fractals* **164**, 112717 (2022)
45. Y. Xie, Z. Yao, X. Hu et al., Enhance sensitivity to illumination and synchronization in light-dependent neurons. *Chin. Phys. B* **30**, 120510 (2021)
46. J.F. Tagne, H.C. Edima, Z.T. Njitacke et al., Bifurcations analysis and experimental study of the dynamics of a thermosensitive neuron conducted simultaneously by photocurrent and thermistance. *Eur. Phys. J. Spec. Top.* **95**, 66 (2022)
47. I. Hussain, D. Ghosh, S. Jafari, Chimera states in a thermosensitive FitzHugh–Nagumo neuronal network. *Appl. Math. Comput.* **410**, 126461 (2021)
48. J. Jia, P. Zhou, X. Zhang et al., Mimic the electric activity in a heat-sensitive membrane in circuit. *AEU-Int. J. Electron. Commun.* **174**, 155069 (2024)
49. C. Rojas, M. Tedesco, P. Massobrio et al., Acoustic stimulation can induce a selective neural network response mediated by piezoelectric nanoparticles. *J. Neural Eng.* **15**, 036016 (2018)
50. V.T. Pham, S. Jafari, S. Vaidyanathan et al., A novel memristive neural network with hidden attractors and its circuitry implementation. *Sci. China Technol. Sci.* **59**, 358–363 (2016)
51. H. Liu, L. Ma, Z. Wang et al., An overview of stability analysis and state estimation for memristive neural networks. *Neurocomputing* **391**, 1–12 (2020)
52. Q. Lai, C. Lai, P.D.K. Kuate et al., Chaos in a simplest cyclic memristive neural network. *Int. J. Bifurc. Chaos* **32**, 2250042 (2022)
53. S. Yang, Z. Guo, J. Wang, Robust synchronization of multiple memristive neural networks with uncertain parameters via nonlinear coupling. *IEEE Trans. Syst., Man, Cybern.: Syst.* **45**, 1077–1086 (2015)
54. F. Parastesh, M. Mehrabbeik, K. Rajagopal et al., Synchronization in Hindmarsh–Rose neurons subject to higher-order interactions. *Chaos: Interdiscipl. J. Nonlinear Sci.* **32**, 013125 (2022)
55. M.S. Anwar, G.K. Sar, M. Perc et al., Collective dynamics of swarmalators with higher-order interactions. *Commun. Phys.* **7**, 59 (2024)
56. M. Ramasamy, S. Devarajan, S. Kumarasamy et al., Effect of higher-order interactions on synchronization of neuron models with electromagnetic induction. *Appl. Math. Comput.* **434**, 127447 (2022)
57. A. Tlaie, I. Leyva, I. Sendiña-Nadal, High-order couplings in geometric complex networks of neurons. *Phys. Rev. E* **100**, 052305 (2019)
58. S. Kundu, D. Ghosh, Higher-order interactions promote chimera states. *Phys. Rev. E* **105**, L042202 (2022)
59. K. Usha, P.A. Subha, Collective dynamics and energy aspects of star-coupled Hindmarsh–Rose neuron model with electrical, chemical and field couplings. *Nonlinear Dyn.* **96**, 2115–2124 (2019)
60. Y. Xie, Z. Yao, J. Ma, Phase synchronization and energy balance between neurons. *Front. Inf. Technol. Electron. Eng.* **23**, 1407–1420 (2022)
61. Y. Wang, G. Sun, G. Ren, Diffusive field coupling-induced synchronization between neural circuits under energy balance. *Chin. Phys. B* **32**, 040504 (2023)
62. J. Sun, C. Li, T. Lu et al., A memristive chaotic system with hypermultistability and its application in image encryption. *IEEE Access* **8**, 139289–139298 (2020)
63. H. Lin, C. Wang, L. Cui et al., Hyperchaotic memristive ring neural network and application in medical image encryption. *Nonlinear Dyn.* **110**, 841–855 (2022)
64. C.L. Li, Z.Y. Li, W. Feng et al., Dynamical behavior and image encryption application of a memristor-based circuit system. *AEU-Int. J. Electron. Commun.* **110**, 152861 (2019)
65. N. Tsafack, A.M. Iliyasu, N.J. De Dieu et al., A memristive RLC oscillator dynamics applied to image encryption. *J. Inf. Secur. Appl.* **61**, 102944 (2021)
66. Y. Guo, F. Wu, F. Yang et al., Physical approach of a neuron model with memristive membranes. *Chaos: Interdiscipl. J. Nonlinear Sci.* **33**, 113106 (2023)
67. F. Yang, J. Ma, G. Ren, A Josephson junction-coupled neuron with double capacitive membranes. *J. Theor. Biol.* **578**, 111686 (2024)
68. F. Yang, Q. Guo, J. Ma, A neuron model with nonlinear membranes. *Cogn. Neurodyn.* **18**, 673–684 (2024)
69. N.F.F. Foka, B. Ramakrishnan, A.C. Chamgoué et al., Neuronal circuit based on Josephson junction actuated by a photocurrent: dynamical analysis and microcontroller implementation. *Eur. Phys. J. B.* **95**, 91 (2022)
70. Y. Zhang, P. Zhou, J. Tang et al., Mode selection in a neuron driven by Josephson junction current in presence of magnetic field. *Chin. J. Phys.* **71**, 72–84 (2021)
71. Y. Zhang, Y. Xu, Z. Yao et al., A feasible neuron for estimating the magnetic field effect. *Nonlinear Dyn.* **102**, 1849–1867 (2020)

Springer Nature or its licensor (e.g. a society or other partner) holds exclusive rights to this article under a publishing agreement with the author(s) or other rightsholder(s); author self-archiving of the accepted manuscript version of this article is solely governed by the terms of such publishing agreement and applicable law.